

Electronic Supplementary Information

Stoichiometric Anion Exchange by Low-Dielectric-Constant Solvent for Highly-Doped Conjugated Polymers with Enhanced Environmental Stability

Daegun Kim^{a,1}, Jiwoo Min^{b,1}, Kyeong-Jun Jeong^{c,1}, Eunsol Ok^b, Jaemin Im^d, Hyun Ho Choi^d, Giwon Lee^e,
Chang Yun Son^{c*} and Kilwon Cho^{b*}

^aSchool of Chemical, Biological and Battery Engineering, Gachon University, Seongnam 13120, Korea.

^bDepartment of Chemical Engineering, Pohang University of Science and Technology, Pohang 37673, Korea.

^cDepartment of Chemistry, Seoul National University, Seoul 08826, Korea

^dDepartment of Materials Engineering and Convergence Technology, Gyeongsang National University, Jinju 52828, Korea

^eDepartment of Chemical Engineering, Kwangwoon University, Seoul 01899, Korea

*Corresponding author.

¹ These authors contributed equally to this work.

Corresponding E-mail: changyunson@snu.ac.kr, kwcho@postech.ac.kr

Table of Contents

Section 1. The solvent properties and stepwise ion-exchange doping

Figure S1. The contact angles of various solvents on the PBTTT surface.

Figure S2. The AFM images PBTTT films after solvent dipping.

Figure S3. Depth XPS spectra of FeCl₃-doped and FeCl₃/DBSA-doped PBTTT films.

Figure S4. GIWAXS results of FeCl₃-doped and FeCl₃/DBSA-doped PBTTT films.

Section 2. Computational analysis of stepwise doping mechanism

Figure S5. Optimized geometries of [BTTT]⁺-[FeCl₄]⁻ pairs in various solvent circumstances.

Figure S6. Optimized geometries of [BTTT]⁺-[BS]⁻ pairs in various solvent circumstances.

Figure S7. Optimized geometries of [BTTT]₃⁺-[FeCl₄]⁻ and [BTTT]₃⁺-[FeCl₄]⁻ pairs.

Figure S8. Energy diagram for the anion exchange in the vicinity of [tri-BTTT]⁺.

Figure S9. Optimized geometries of [tri-BTTT]⁺-[FeCl₄]⁻ pairs in various solvent circumstances.

Figure S10. Optimized geometries of [tri-BTTT]⁺-[BS]⁻ pairs in various solvent circumstances.

SI Section 1. The solvent properties and stepwise ion-exchange doping

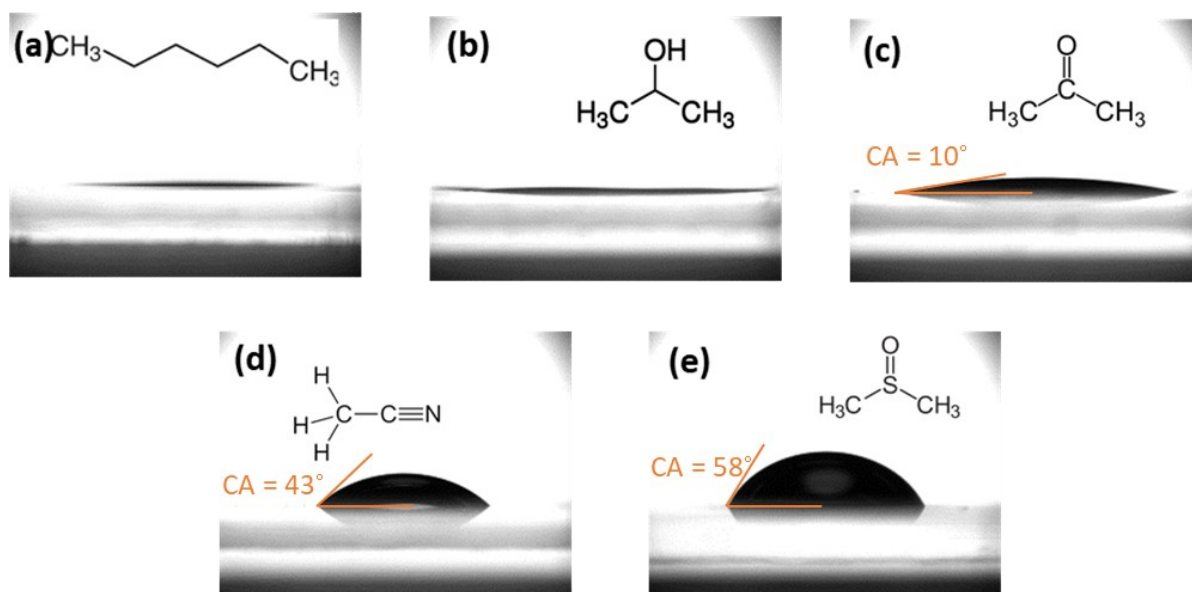


Figure S1. The contact angle of (a) HEX, (b) IPA, (c) ACT, (d) ACN, and (e) DMSO on PBTTT films.

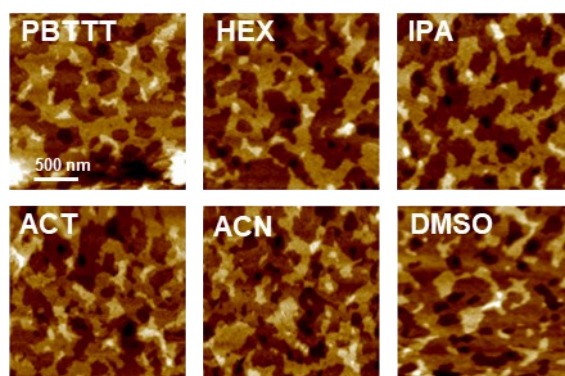


Figure S2. The AFM images of PBTTT films after dipping in HEX, IPA, ACT, ACN, and DMSO for 1 hr.

The label PBTTT indicates the film surface without the solvent dipping.

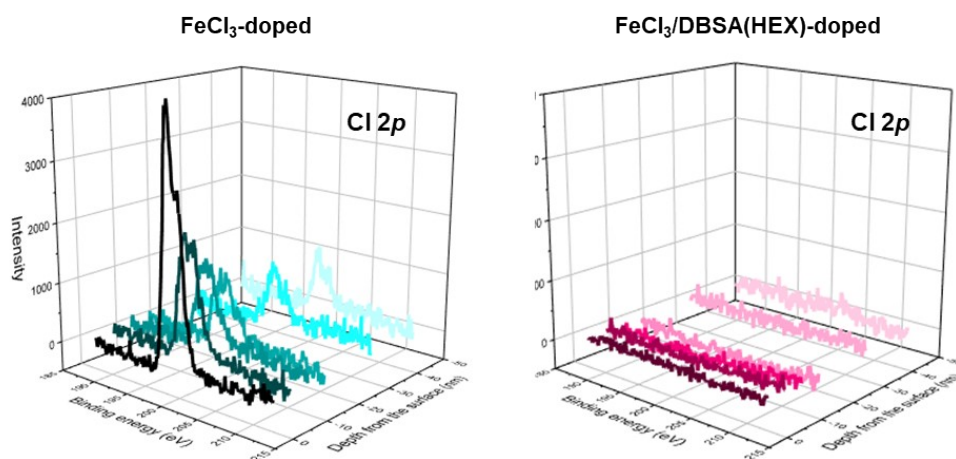


Figure S3. Depth XPS Cl 2p spectra of FeCl₃-doped and FeCl₃/DBSA(HEX)-doped PBTTT films. FeCl₃ was doped using ACN as the solvent.

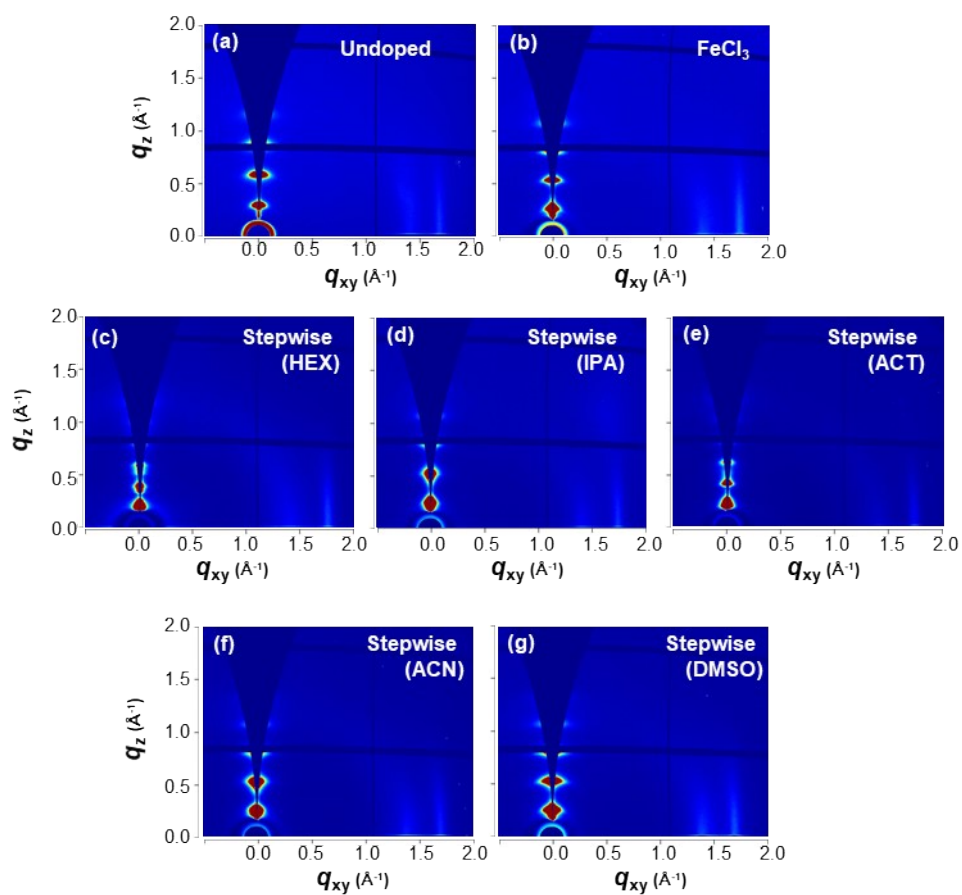


Figure S4. GIWAXS patterns of undoped, FeCl₃-doped and FeCl₃/DBSA-doped with various solvents. FeCl₃ was doped using ACN as the solvent.

SI Section 2. Computational analysis of stepwise doping mechanism

2-1. Density functional theory (DFT) calculation details

DFT calculations were performed on the Gaussian 09 package.^[1] The level of theory was B3LYP functional with 6-31+G(d,p) basis sets.^[2, 3] The effect of solvents were taken into account implicitly through the integral equation formalism polarizable continuum model (IEFPCM).^[4] In intermolecular binding energy calculations, basis set superposition error (BSSE) was corrected by the counterpoise method.^[5] We used the convention that attractive intermolecular binding energy corresponds to a negative sign according to the formula below:

$$\Delta E_{\text{bind(AB)}} = E_{\text{AB}} - (E_{\text{A}} + E_{\text{B}}), \quad (6)$$

where E_{A} , E_{B} , and E_{AB} are the calculated system total energies for the monomers of species A, species B, and the coexistent A-B dimer, respectively.

For computational efficiency and circumventing the system energy fluctuations by conformational movements of hydrocarbon tailgroups, we used surrogate molecules C₀-BTTT monomer (notated as BTTT) and benzenesulfonic acid (BSA) to represent the PBTTT polymer and DBSA, respectively (**Figure S5** and **S6**). The polaron of PBTTT was modeled as a radical cation [BTTT]⁺, which possesses one unpaired electron and (+1) charge within a truncated BTTT monomer unit.

The electrostatic potential (ESP) at the vicinity of polaron-dopant anion pairs were calculated by the Gaussian 09 *cubegen* utility using the density matrices with optimized geometries in HEX implicit solvent. ESP distributions were visualized as a color-coded isosurface at total electron density of 0.01 e bohr⁻³ in the color range from -0.15 to 0.15 atomic units (a.u.).

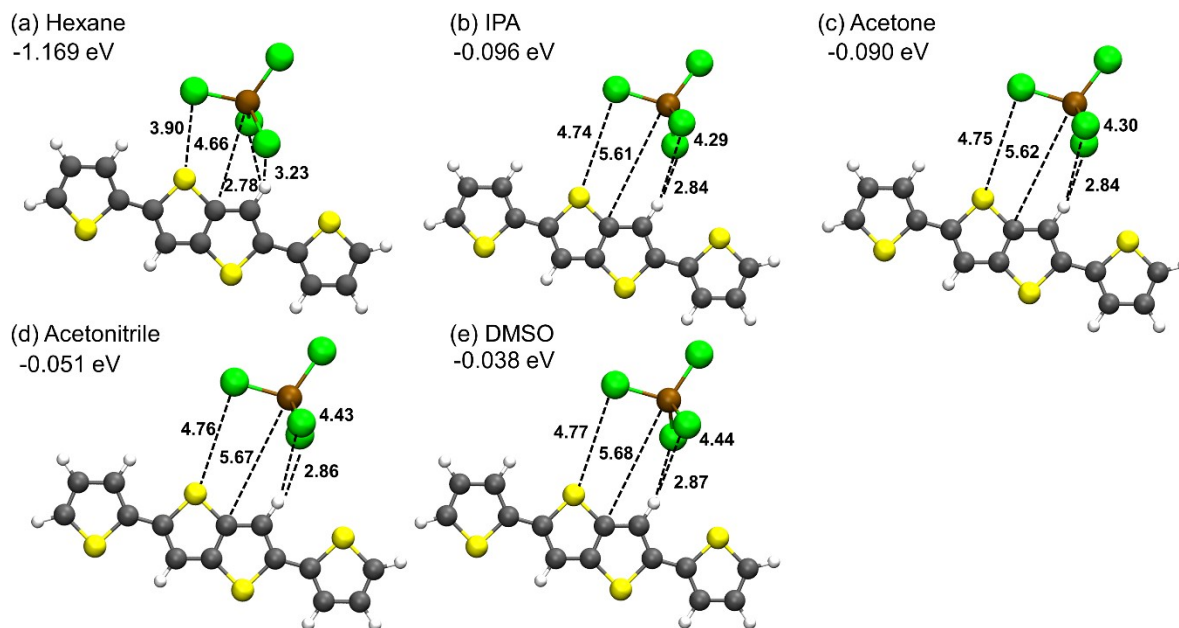


Figure S5. Optimized geometries and binding energies of [BTTT]⁺ (monomer polaron) pairing with [FeCl₄]⁻ in (a) HEX, (b) IPA, (c) ACT, (d) ACN and (e) DMSO implicit solvents in DFT calculation. Interatomic distances are shown by the dotted lines in unit of Å.

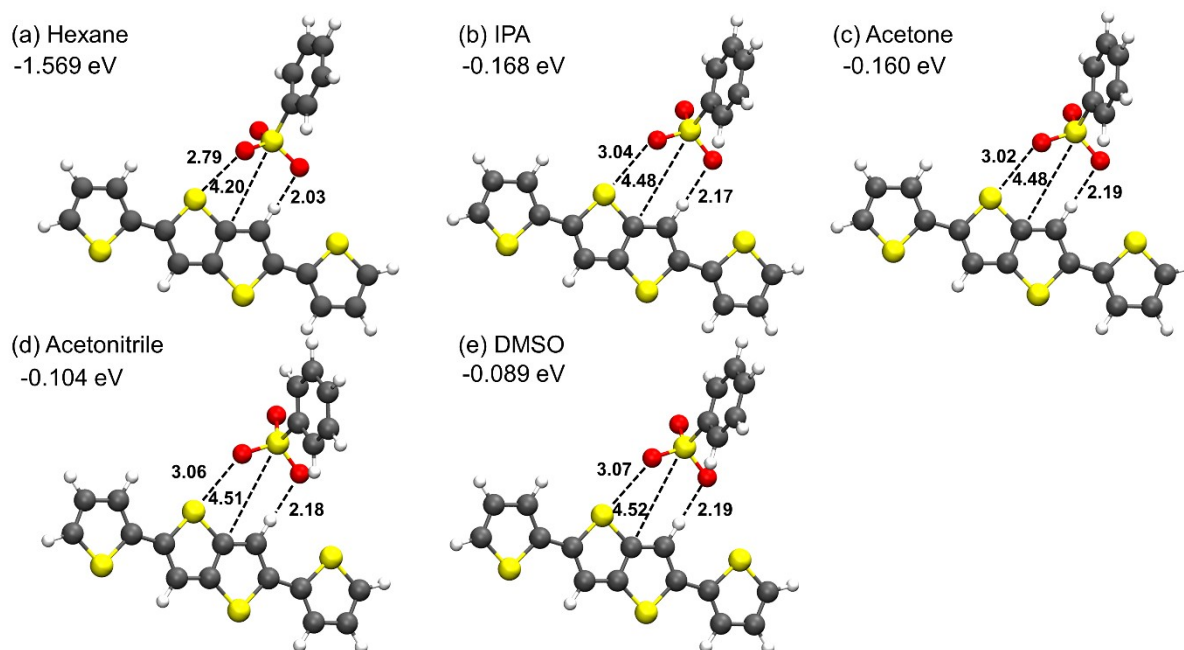


Figure S6. Optimized geometries and binding energies of [BTTT]⁺ (monomer polaron) pairing with [BSA]⁻ in (a) HEX, (b) IPA, (c) ACT, (d) ACN and (e) DMSO implicit solvents in DFT calculation. Interatomic distances are shown by the dotted lines in unit of Å.

2-2. DFT calculations of stacked BTTT triple layer polaron - dopant anion binding pair

In our simplest representation in DFT calculations, the BTTT polaron stands alone, potentially allowing the dopant anion to approach the flat plane of the ring structures. This binding orientation is forbidden in the real system due to the π -stacked structure of PBTTT backbones. To verify that the open space normal to the BTTT ring plane in our model does not mislead the dopant anion exchange mechanism, we also performed DFT calculations for the binding geometries and energies of the dopant anions on a π -stacked triple layer of BTTT with one polaron located in the middle (Figure S7). In these calculations, the BTTT triple layer was generated by replicating the optimized BTTT monomer geometry with π -stacking distance of 3.53 Å. The designated interlayer spacing is based on our GIWAXS measurement along the q_{xy} direction for the FeCl₃-doped PBTTT film, indicating a peak at 1.78 Å⁻¹ after 3 minutes of doping. The geometries were optimized with fixing the BTTT triple layer and only allowing the dopant anion to move. In HEX, the binding orientations were consistent to those predicted with stand-alone BTTT polaron monomer; the dopant anions were located on the side of [BTTT]⁺ thienothiophene ring. The binding energy of [BS]⁻ was more negative than [FeCl₄]⁻, agreeing with the trend of binding energies on [BTTT]⁺ monomer. This supports that the explanations of ion exchange mechanism based on the computational results with [BTTT]⁺ monomer is valid.

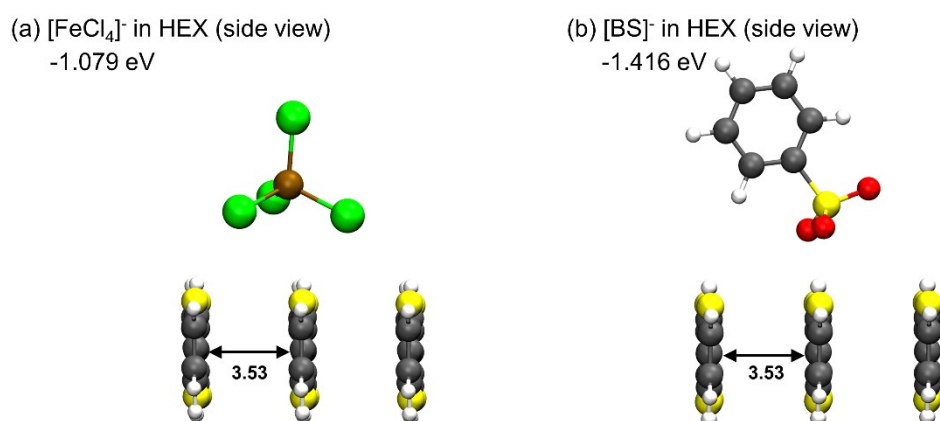


Figure S7. Optimized geometries and binding energies of π -stacked [BTTT]₃⁺ (one polaron in the middle of the triple layer) pairing with (a) [FeCl₄]⁻ and (b) [BS]⁻ in HEX implicit solvent in DFT calculation in a side view.

2-3. DFT calculations of BTTT trimer polaron – dopant anion binding pair

Our simplest computational model assumed one dopant molecule was bound to one monomer of the conjugated polymer (CP), and thereby possessing one charge carrier. If every monomer unit of CP contains polaron, we estimated that hypothetical charge carrier density will be $n = 8.9 \times 10^{20} \text{ cm}^{-3}$ regarding the reported unit cell parameters^[6, 7]. According to our charge carrier density measurements, the assumption of one charge carrier per every CP monomer overestimates n , and 3-5 monomers were likely to hold one charge carrier in real system. To verify the truncation of CP as monomer was relevant, we examined whether any unvisited physical trends exist by incorporating adjacent neutral BTTT monomers connected to the oxidized BTTT monomer. Therefore, by DFT calculations, we also examined the binding geometries and energies of polaron-dopant anion pairs based on BTTT trimers, notated as $[\text{tri-BTTT}]^+$ (**Figure S8-S10**). To mitigate the large computational cost, in these BTTT trimer calculations, the polaron-dopant anion pair geometries were optimized with constraining $[\text{tri-BTTT}]^+$ to their optimized geometry without dopants. The binding motifs and qualitative trends in energies with respect to solvent dielectric constants were consistent to those predicted with BTTT monomer models, supporting that the computational results with BTTT monomer representations were relevant enough to examine the molecular mechanism and solvent effect on ion exchange.

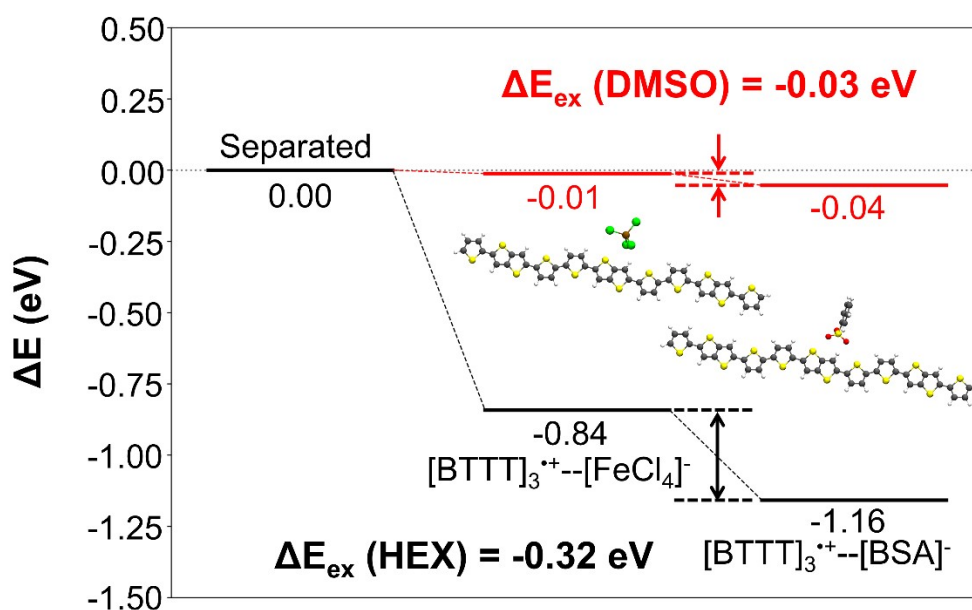


Figure S8. Energy diagram for the dopant ion exchange in the vicinity of [tri-BTTT]⁺ (trimer polaron) in HEX (black line) and DMSO (red line) predicted by DFT.

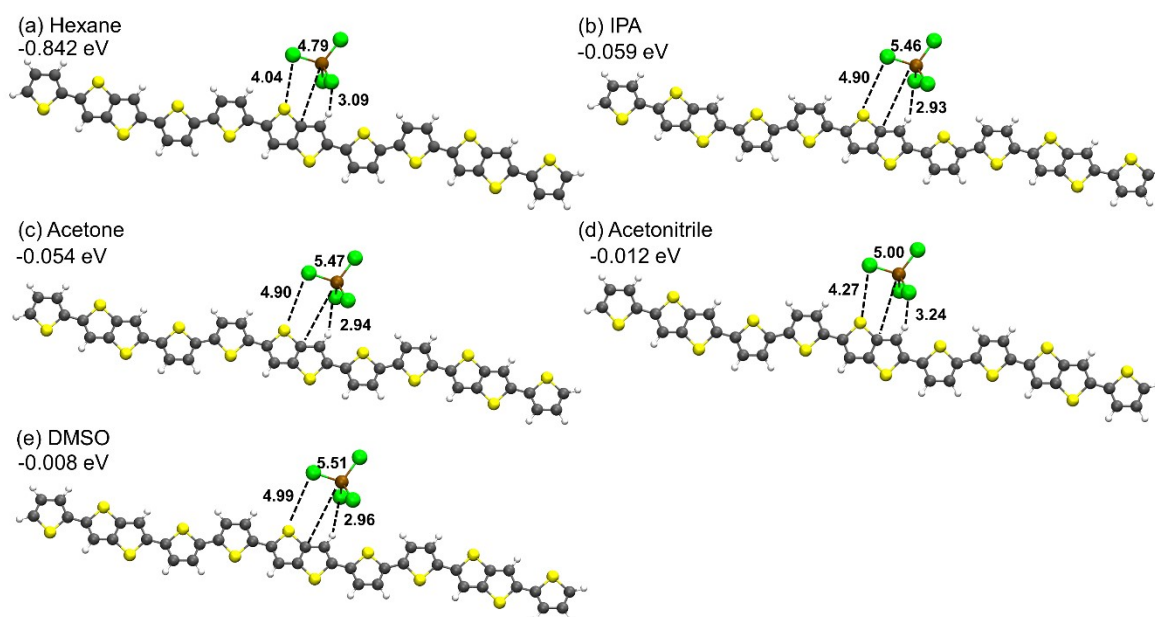


Figure S9. Optimized geometries and binding energies of [tri-BTTT]⁺ (trimer polaron) pairing with [FeCl₄]⁻ in (a) HEX, (b) IPA, (c) ACT, (d) ACN and (e) DMSO implicit solvents in DFT calculation. Interatomic distances are shown by the dotted lines in unit of Å.

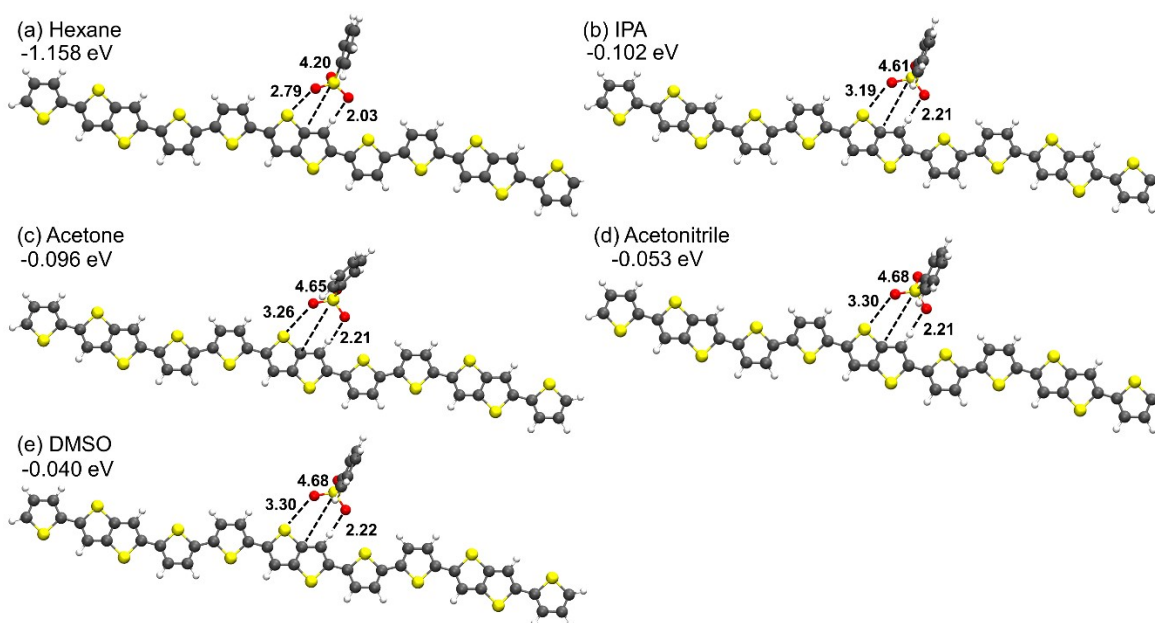


Figure S10. Optimized geometries and binding energies of [tri-BTTT]⁺ (trimer polaron) pairing with [BS]⁻ in (a) HEX, (b) IPA, (c) ACT, (d) ACN and (e) DMSO implicit solvents in DFT calculation. Interatomic distances are shown by the dotted lines in unit of Å.

References

- [1] C. Bordes, V. Fréville, E. Ruffin, P. Marote, J.Y. Gauvrit, S. Briançon, P. Lantéri, Determination of poly(ϵ -caprolactone) solubility parameters: Application to solvent substitution in a microencapsulation process, *Int. J. Pharm.* 2010, **383**, 236–243.
- [2] L. Snyder, Classification of the solvent properties of common liquids, *J. Chromatogr. Sci.*, 1978, **16**, 223–234.
- [3] B. Kratochvil, P.F. Quirk, Ferrocene as a primary standard for oxidation-reduction titrations in acetonitrile, *Anal. Chem.*, 1970, **42**, 492–495.
- [4] M.J. Frisch, G.W. Trucks, H.B. Schlegel, G.E. Scuseria, M.A. Robb, J.R. Cheeseman, G. Scalmani, V. Barone, G.A. Petersson, et al., Gaussian 09, Revision A.02, Gaussian, Inc., Wallingford, CT, 2010.
- [5] C. Lee, W. Yang, R.G. Parr, Development of the Colle-Salvetti correlation-energy formula into a functional of the electron density, *Phys. Rev. B*, 1988, **37**, 785–789.
- [6] A.D. Becke, Density-functional thermochemistry. III. The role of exact exchange, *J. Chem. Phys.*, 1993, **98**, 5648–5652.
- [7] E. Cancès, B. Mennucci, J. Tomasi, A new integral equation formalism for the polarizable continuum model: Theoretical background and applications to isotropic and anisotropic dielectrics, *J. Chem. Phys.*, 1997, **107**, 3032–3041.
- [8] S.F. Boys, F. Bernardi, The calculation of small molecular interactions by the differences of separate total energies. Some procedures with reduced errors, *Mol. Phys.*, 1970, **19**, 553–566.
- [9] J. Li, Y. Zhao, H.S. Tan, Y. Guo, C.-A. Di, G. Yu, Y. Liu, M. Lin, S.H. Lim, Y. Zhou, H. Su, B.S. Ong, A stable solution-processed polymer semiconductor with record high-mobility for printed transistors, *Sci. Rep.*, 2012, **2**, 754.
- [10] D. Venkateshvaran, M. Nikolka, A. Sadhanala, V. Lemaire, M. Zelazny, M. Kepa, M. Hurhangee, A.J. Kronemeijer, V. Pecunia, I. Nasrallah, I. Romanov, K. Broch, I. McCulloch, D. Emin, Y. Olivier, J. Cornil, D. Beljonne, H. Sirringhaus, Approaching disorder-free transport in high-mobility conjugated polymers, *Nature*, 2014, **515**, 384–388.